F. S. Henry
Molecular and Integrative Physiological Sciences,
Department of Environmental Health,
Harvard School of Public Health,
Boston, MA 02115

S. Haber
Faculty of Mechanical Engineering,
Technion-Israel Institute of Technology,
Haifa, Israel

D. Haberthür
Swiss Light Source,
Paul Scherrer Institut,
Villigen, Switzerland

N. Filipovic
Molecular and Integrative Physiological Sciences,
Department of Environmental Health,
Harvard School of Public Health,
Boston, MA 02115;
Faculty of Mechanical Engineering,
University of Kragujevac, Serbia

D. Milasinovic
Faculty of Mechanical Engineering,
University of Kragujevac, Serbia

J. C. Schittny
Institute of Anatomy,
University of Bern
Bern, Switzerland

A. Tsuda[1]
Molecular and Integrative Physiological Sciences,
Department of Environmental Health,
Harvard School of Public Health,
Boston, MA 02115
e-mail: atsuda@hsph.harvard.edu

The Simultaneous Role of an Alveolus as Flow Mixer and Flow Feeder for the Deposition of Inhaled Submicron Particles

In an effort to understand the fate of inhaled submicron particles in the small sacs, or alveoli, comprising the gas-exchange region of the lung, we calculated the flow in three-dimensional (3D) rhythmically expanding models of alveolated ducts. Since convection toward the alveolar walls is a precursor to particle deposition, it was the goal of this paper to investigate the streamline maps' dependence upon alveoli location along the acinar tree. On the alveolar midplane, the recirculating flow pattern exhibited closed streamlines with a stagnation saddle point. Off the midplane we found no closed streamlines but nested, funnel-like, spiral, structures (reminiscent of Russian nesting dolls) that were directed towards the expanding walls in inspiration, and away from the contracting walls in expiration. These nested, funnel-like, structures were surrounded by air that flowed into the cavity from the central channel over inspiration and flowed from the cavity to the central channel over expiration. We also found that fluid particle tracks exhibited similar nested funnel-like spiral structures. We conclude that these unique alveolar flow structures may be of importance in enhancing deposition. In addition, due to inertia, the nested, funnel-like, structures change shape and position slightly during a breathing cycle, resulting in flow mixing. Also, each inspiration feeds a fresh supply of particle-laden air from the central channel to the region surrounding the mixing region. Thus, this combination of flow mixer and flow feeder makes each individual alveolus an effective mixing unit, which is likely to play an important role in determining the overall efficiency of convective mixing in the acinus. [DOI: 10.1115/1.4007949]

Keywords: lung flow, acinar fluid mechanics, submicron particle, chaotic mixing, particle transport and deposition, gas phase, alveolation

Introduction

Gas exchange occurs in the numerous small sacs, or alveoli, that make up the pulmonary acinus (e.g., see Haefeli-Bleuer and Weibel [1]). With each new breath of air, millions of submicron particles are carried into the acinar region, and a small fraction of these particles deposit on the gas-exchange surfaces of the alveoli (e.g., see ICRP [2]). Knowledge of particle deposition mechanics in the acinus is important for the understanding of the beneficial effects of inhaled therapeutic drug therapies, and the deleterious effects of airborne pollutants. In this paper we consider flow patterns in 3D model alveoli and how these patterns may bring aerosol particles sufficiently close to the surface from which position they may deposit by diffusion, inertia, or gravity.

In previous studies of acinar fluid mechanics, we found experimentally that the presence of recirculating flow in an alveolus plays a significant role in acinar flow mixing [3–5]. Our associated numerical studies revealed that tidal alveolar flows with recirculating flow patterns are chaotic [6–10]. This finding led to the concept of chaotic mixing (i.e., flow-induced mixing), which may occur in the acinus [4,11]. Recently, numerous experimental [12–16] and numerical studies [17–22] of acinar flows have appeared in the literature, and many of these have confirmed the presence of recirculating alveolar flow. The occurrence of chaotic, or convective, mixing in the acinus is particularly interesting because no flow-induced mixing was assumed to occur in the classical descriptions of acinar flows [23]. This conclusion was based on the fact that the Reynolds number of the flow is very low, and hence it was thought that transport in the acinus was completely dominated by diffusion [24,25].

All of the above studies used idealized models of acinar airways but recent advances in imagining technology has made possible the construction and computational fluid dynamics (CFD) analysis of realistic models of alveolated ducts [26,27]. Specifically, using synchrotron radiation-based X-ray tomographic microscopy (SRXTM), part of an acinus can now be imaged in sufficient detail to allow the construction of an accurate geometric model of a cluster of alveoli [28–30]. In the following we describe briefly the process by which the images were made. Rat lung samples were prepared according to Tschanz et al. [31] and Luyet et al. [32]. To extract multiple alveolar ducts we [29] performed SRXTM wide-field scans for a sample volume of approximately $3.0 \times 4.2 \times 4.2$ mm^3 at a voxel size of 1.48 μm^3. The tomographic imaging was performed on the TOMCAT beamline at the Swiss Light Source at the Paul Scherrer Institute in Vilgen, Switzerland [33]. The medial lower tip of the right lower lobe of the lung of a Sprague Dawley rat was imaged and three-dimensional segmentation

[1]Corresponding author.

Contributed by the Bioengineering Division of ASME for publication in the JOURNAL OF BIOMECHANICAL ENGINEERING. Manuscript received February 27, 2012; final manuscript received October 13, 2012; accepted manuscript posted October 25, 2012; published online November 27, 2012. Assoc. Editor: Dalin Tang.

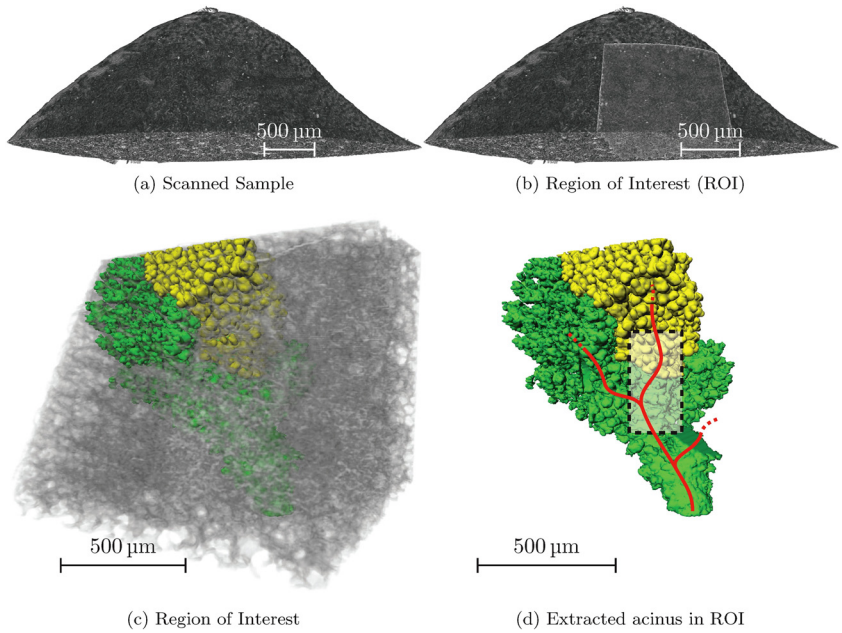

Fig. 1 Workflow to extract acinar duct: (*a*) Wide-field scanned sample of the tip of the right lower lung lobe of a Sprague-Dawley rat. (*b*) Region of interest (ROI) where we extracted one small acinus superimposed on sample (small cube with white border). (*c*) Rotated close-up view of the ROI, including two separate airways segments extracted using a threshold interval based region growing. Since the ROI is rotated in comparison to (*b*), the scale bars are of slightly different length. (*d*) Isosurfaces of extracted airway segments. A part of a single acinus (yellow, or light grey) and adjoining airway segment (green, or dark grey) in ROI. Several parts of the airway segment have been removed for clarity. The approximate path of the center of the airway may be discerned in the semitransparent rectangle, which marks the approximate region of one alveolar duct.

was performed using MeVisLab (version 2.1, MeVis Medical Solutions AG and Fraunhofer MEVIS, Institute for Medical Image Computing, Bremen, Germany). The imaged section contains multiple acini (workflow to extract them is shown in Fig. 1).

Before considering the details of alveolar flow patterns in more idealized 3D model alveoli, we performed an exploratory numerical analysis in a high-resolution geometric moving-wall model of a thoroughfare duct with realistic alveoli. This was done to confirm that recirculating flow occurs in the acinus and that it is not an artifact of the idealization process. The model was constructed from images gained using the process described above. A 3D mesh was constructed using a finite element volume meshing technique developed previously for CFD [28]. A part of the segmented region was removed and inlet and outlet ducts were added to the alveolated segment (Fig. 2). In other words, this model was essentially a thoroughfare duct with partially alveolated walls. The time-dependent 3D airflow was defined by Navier-Stokes equations and solved numerically on a moving mesh using a finite element code [34]. The alveoli and the adjacent airway were assumed to expand and contract simultaneously in a self-similar fashion during breathing. Figure 3 depicts the flow inside these constructed alveoli at peak inspiratory flow, with $\mathrm{Re}_{\mathrm{duct}} = 1.5$. Frames (*a*) and (*b*) show closed recirculating flows in the middle of alveolar cavity, frame (*c*) depicts spiral flow patterns from the midplane of the alveolus toward the expanding walls, frame (*d*) focuses on incoming flow from the central channel, and finally, frame (*e*) is a combination of flows shown in (*c*) and (*d*).

Having confirmed that recirculation is likely to occur in the acinus, we will consider, briefly, the mechanics of deposition. We show below that the convective transport provided by recirculation is a necessary first step to the deposition of submicron particles. To determine particle deposition locations, particle motion from the airway into the alveolus and its consecutive motion inside the alveolus must be explored. The main forces that govern the motion of the inhaled particles are hydrodynamic drag, Brownian, inertia, and gravity. The hydrodynamic drag force exerted on small particles will cause particles to convect closely along fluid pathlines, while the other forces cause particle trajectories to cross them. Thus, particle trajectories are determined by the relative magnitude of these forces. The dimensionless parameters that govern the relative importance of convection to diffusion, inertia to convection and gravity to convection are the Peclet (Pe), Stokes (St), and gravity (G) numbers [35], respectively, defined as follows:

$$\mathrm{Pe} = VD_{aw}/D_{\mathrm{diff}}, \quad \mathrm{St} = \pi\rho_p D^2/(18\mu T), \quad G = \pi\rho_p g D^2/(18\mu V)$$

where V is the duct mean velocity of air in the airway, D_{aw} is the airway diameter, D is the particle diameter, ρ_{p} is the particle density (assumed to be 1 g/cm^3), T is the breathing period, μ is the viscosity, g is the gravity acceleration, and D_{diff} is the diffusion coefficient.

Since most of the larger particles settle on the airway walls leading to the acinus, we focus on the fate of submicron particles, e.g., particles between 0.01 and 1 μm in diameter. Table 1 provides the values of the foregoing dimensionless parameters calculated for three particle sizes at different locations along the acinar tree. The breathing period of $T = 4$ s was assumed and velocity values are quoted from Pedley et al. [36] for inhalation rate of 0.5 liters/s along the acinar tree.

The large Peclet numbers, together with the small Stokes and gravity numbers indicate that submicron particle trajectories essentially follow fluid pathlines. In other words, the main form of transport for these particles is convection. If the inhalation rate were increased to a physiological feasible level of 5 liters/s, the foregoing conclusion would not change with the exception of the relative importance of gravity for micron size particles in the 22nd generation.

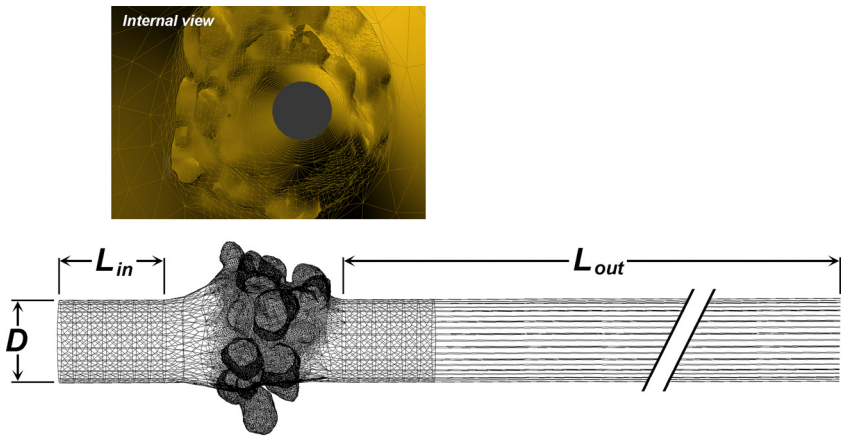

Fig. 2 Geometric model of a thoroughfare duct with partially alveolated walls imaged by SRXTM. The time-dependent, three-dimensional, Navier-Stokes equations were solved on a moving mesh using a finite element code that incorporated the arbitrary Lagrangian-Eulerian formulation for moving meshes. The geometrical model was developed using the C++ object oriented programming language and OpenGL graphic library [34]. The system of discrete equations was solved using a nonsymmetric Gaussian solver. About 400,000 eight-node, hexahedral, finite elements were employed with eight unknown velocities and constant pressure over the element. The actual pressure field was calculated at the post-processing stage. Mesh independence was reached at 400,000 to 600,000 finite elements with an error of less than 0.1% in an average difference for the velocity field. Time step independence was achieved at 400 time steps per cycle. A Laplacian smoothing technique was used in constructing the realistic alveolar model to create a smooth surface after the image reconstruction process. For each calculation, a parallel version of the solver required 24 h on 40 parallel Intel core2quad q6600, 2.4 GHz, processors. The size of the alveoli is 80 μm in diameter on average.

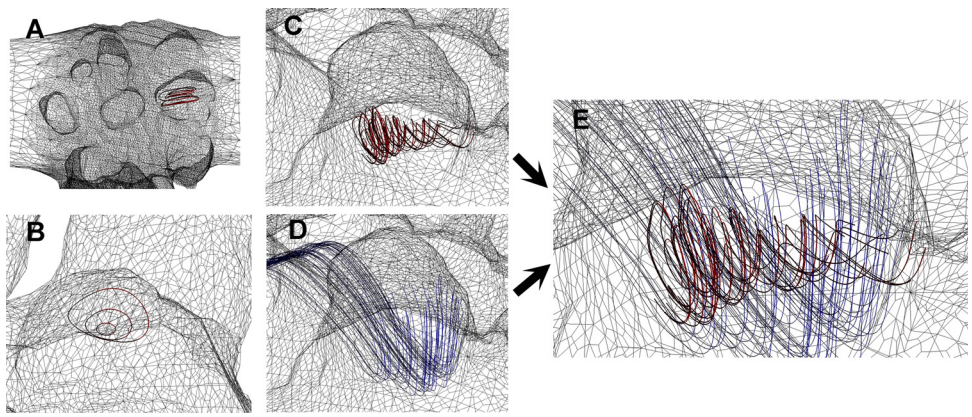

Fig. 3 Peak inspiration alveolar flow patterns at $Re_{duct} = 1.5$ in a geometric model of a thoroughfare duct with partially alveolated walls (Fig. 2). (*a*) and (*b*) Closed recirculating flows in the middle of alveolar cavity. (*c*) Spiral flow patterns from the midplane of the alveolus toward the expanding walls. (*d*) Incoming flow from the central channel. (*e*) Flows of (*c*) and (*d*) combined. The size of the alveoli is 80 μm in diameter on average.

For the purposes of discussion, submicron particle deposition can be described as a two-stage process. During the first stage, particles are governed by the hydrodynamic drag force and hence follow closely fluid pathlines. Thus, like the flow, submicron particles follow rotational trajectories in the alveolus. For those particles that come in close proximity to the alveolar surface, a second stage becomes necessary. This is because convection can only bring the particles close to the surface but cannot cause direct particle deposition (wall effects result in a drag force that becomes exceedingly large). Hence, for deposition, a force is needed to displace the particles from the flow pathlines, and this may be provided by particle diffusion, inertia, or gravity. We note that in reality both stages occur simultaneously. That is, diffusion, inertia, and gravity act on the particle at all times and cause the particle to stray very slightly from the fluid pathline over the whole of the breathing cycle but this small difference only becomes important when the particle is in extremely close proximity to the wall.

The objective of this current work is to explain how the complex, 3D, flow structure within an alveolus—especially off midplane—can bring submicron particles from the central acinar airway to the vicinity of the alveolar surface. An idealize geometric model of the alveolus and its adjacent airway are constructed as a single spherical cap, which opens into a short section of a circular duct and low Reynolds number flow analysis was performed numerically as follows.

Table 1 Dimensionless parameters, gravity (*G*), Peclet (Pe), Stokes (St) for three particle sizes, and airflow Reynolds (Re) numbers calculated at three different locations along the acinar tree during normal breathing

G[a]	St[a,b]	Pe	Re[c]	D_{diff} (m^2/s)	D (μm)	V (m/s)[d]	D_{aw} (mm)[e]	Generation
2.22×10^{-7}	2.20×10^{-10}	3.60×10^{2}	1.17×10	5.40×10^{-8}	0.01	0.039	0.50	16
2.22×10^{-5}	2.20×10^{-8}	2.82×10^{4}	1.17×10	6.90×10^{-10}	0.1	0.039	0.50	
2.22×10^{-3}	2.20×10^{-6}	7.20×10^{5}	1.17×10	2.70×10^{-11}	1	0.039	0.50	
5.69×10^{-7}	2.20×10^{-10}	1.12×10^{2}	3.66×10^{-1}	5.40×10^{-8}	0.01	0.015	0.40	18
5.69×10^{-5}	2.20×10^{-8}	8.80×10^{3}	3.66×10^{-1}	6.90×10^{-10}	0.1	0.015	0.40	
5.69×10^{-3}	2.20×10^{-6}	2.25×10^{5}	3.66×10^{-1}	2.70×10^{-11}	1	0.015	0.40	
1.84×10^{-6}	2.20×10^{-10}	3.12×10^{1}	1.02×10^{-1}	5.40×10^{-8}	0.01	0.005	0.36	20
1.84×10^{-4}	2.20×10^{-8}	2.44×10^{3}	1.02×10^{-1}	6.90×10^{-10}	0.1	0.005	0.36	
1.84×10^{-2}	2.20×10^{-6}	6.25×10^{4}	1.02×10^{-1}	2.70×10^{-11}	1	0.005	0.36	
5.47×10^{-6}	2.20×10^{-10}	9.07×10	2.95×10^{-2}	5.40×10^{-8}	0.01	0.002	0.31	22
5.47×10^{-4}	2.20×10^{-8}	7.10×10^{2}	2.95×10^{-2}	6.90×10^{-10}	0.1	0.002	0.31	
5.47×10^{-2}	2.20×10^{-6}	1.81×10^{4}	2.95×10^{-2}	2.70×10^{-11}	1	0.002	0.31	

[a]$\rho_p = 1000$ kg/m^3, $\mu = 1.98 \times 10^{-5}$ kg/ms.
[b]$T = 4$ s.
[c]$\text{Re} = VD_{aw}/\nu$, $\nu = 1.66 \times 10^{-5}$ m^2/s.
[d]Based on an inhalation flow rate of 0.5 liters/s.
[e]Values taken from Table 2 of Weibel et al. 2005 [37].

Method

Geometric Model. Assume that the alveolated channel can be divided into small units each of which comprising a cylindrical straight tube (central channel) and a spherical cap (alveolus) (Fig. 4). The diameter of the central channel was set to 0.325 mm, which represent the weighted average of the duct diameters in generations 15 through 18 in adult human [37]. As the depth of the alveolus is of the same order as the duct diameter [38] we set the diameter of alveolus equal to the duct diameter. The duct length was set to three duct diameters, which, because of the very low value of Reynolds number, was sufficient to ensure fully developed Poiseuille flow at the alveolar opening. The distance of the center of the sphere from the central channel wall was adjusted so that the alveolar opening angle was 120 deg (equivalent to the 5/6th sphere model of Weibel [38]). Note that the configuration of this model is similar to the one that Sznitman et al. [21] studied. However, our focus is on the flow structure off midplane (described below), which was unclear and not discussed by Sznitman et al. [21].

Boundary Conditions. We assumed that the alveoli expand and contract in a geometrically similar fashion, that is, all length scales change as $L(t) = LF(t)$, where $F(t) = 1 + K \sin nt$, $K = (\phi - 1)/(\phi + 1)$, $\varphi = (1 + C)^{1/3}$, $C = V_T/V_{\min}$, $n = 2\pi/T$,

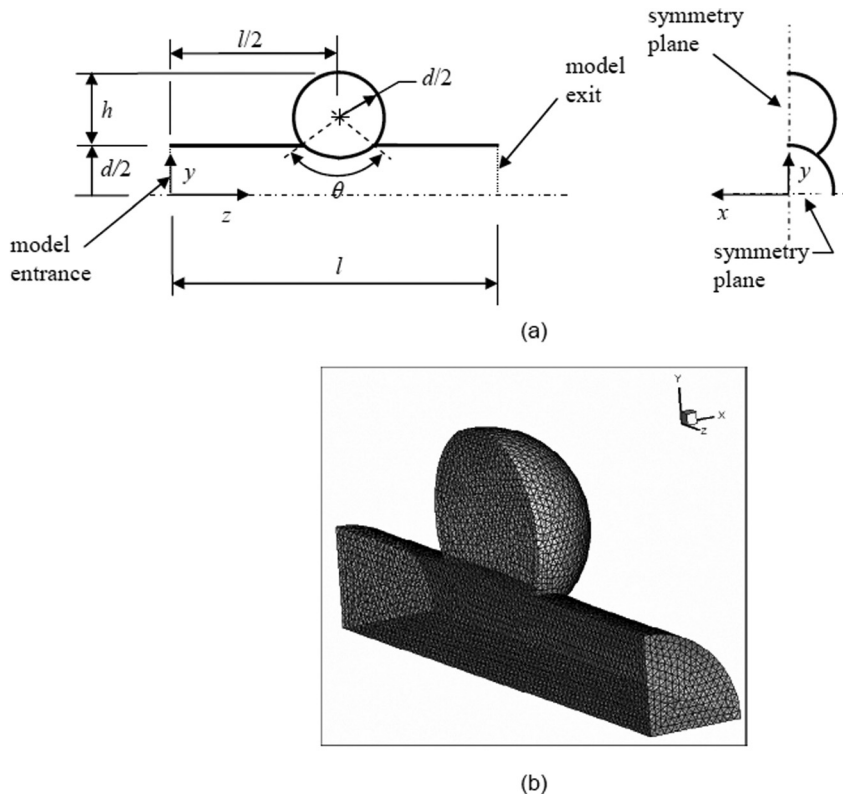

Fig. 4 (*a*) Geometrical details of the idealized CFD model, where *d* is the diameter of the central duct and the alveolus, *l* is the duct length, and $h = 3\,d/4$ for an opening angle $\theta = 120$ deg. The main flow direction is aligned with the *z* direction and the midplane of the alveolus is a *y-z* plane at $x = 0$. (*b*) Typical grid with 80,327 tetrahedral cells.

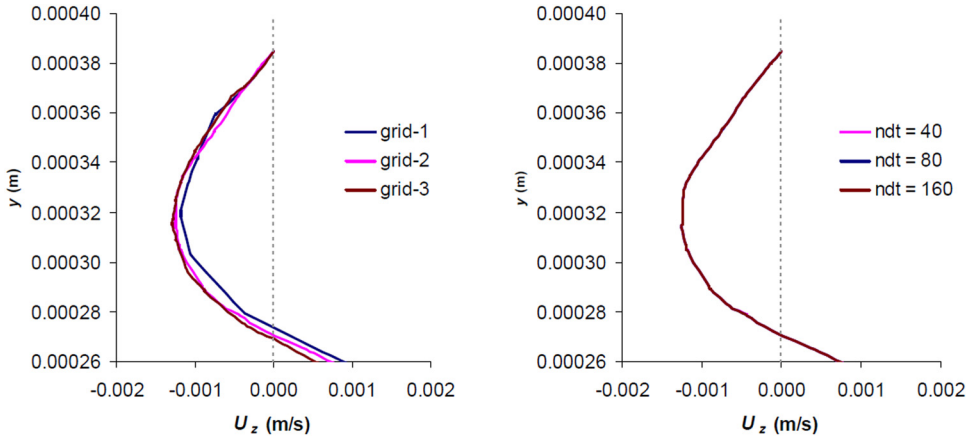

Fig. 5 Axial velocity profile at maximum inspiratory flow at $x = 0$ and $z = 0$ over the top half of the model alveolus for three different grids (left) and three different time steps (right). (Grid 1, 2, and 3 = 41,625, 80,327, and 181,882 cells, respectively, and *ndt* = number of time steps over the breathing cycle.)

V_T is the tidal volume, $V_{\min}$ is the minimum lung volume, T is the breathing period, and the over bar signifies the mean value. Here C and T were set to 0.2 and 4 s, respectively. These values correspond to normal breathing in humans. Acinar ductal flow is characterized by the Reynolds number Re of the central channel flow. The flow pattern inside the alveolar cavity can be characterized by the ratio of the flow entering the alveolus to that passing by in the central channel Q_A/Q_D [6,7,12,18,21]. However, these two parameters cannot be defined independently as Re is a function of Q_D. We defined the maximum Reynolds number as $\mathrm{Re}_{\max} = U_{\max}\bar{d}/\nu$, where $U_{\max}$ is the maximum bulk velocity at the duct inlet, $\bar{d}$ is the mean diameter of the duct, and ν is the kinematic viscosity. It can be shown that at the model inlet $U = 3(\bar{V}_M + \bar{V}_D)/\bar{A}dF/dt$, where $\bar{A}$ is the time-mean flow area of the central channel $\bar{V}_M$ is the time-mean model volume and $\bar{V}_D$is the time-mean value of the acinar air volume distal of the model. (Namely, the part of the lung that is fed by the airflow passing through the model duct.) Hence, $U_{\max} = 6\pi(K/T)(\bar{V}_M + \bar{V}_D)/\bar{A}$. Thus, we see that the Reynolds number is linearly related to K, which is a function of the tidal volume, and inversely related to the breathing period T.

The velocity distribution at the duct inlet is not actually known. Also, it cannot exactly be calculated unless the flow inside the whole lung is calculated simultaneously. (This is due to the elliptic form of the governing differential equations.) With current computer capacity, such an endeavor is presently not feasible. We believe that the flow reaches a nearly "fully developed" state (i.e., a Poiseuille distribution) within a small downstream distance from the alveolus mouth, due to the very low Reynolds number governing the flow. Thus, this downstream Poiseuille flow distribution can be used as the upstream distribution for the next alveolus, etc. essentially separating the lung into many small unit cells consisting of a small straight airway and a single alveolus protruding from it.

Numerical Approach. The flow in the model was simulated by solving the Navier-Stokes equations on a moving mesh using ANSYS FLUENT (Ansys Inc., Canonsburg, PA, USA). At the distal boundary (the outlet), the pressure was set to zero. At the proximal boundary (the inlet), the time varying bulk velocity U was defined. The Reynolds number is so low for these flows that it can be expected that the flow becomes fully developed in less than one duct diameter [39] and hence, the details of the velocity profile at the flow boundaries will not affect the flow in the alveolus. The value of $\bar{V}_D$ was adjusted to achieve the required values of Q_A/Q_D and $\mathrm{Re}_{\max}$, which defined the location of the model in the acinar tree.

Grids of increasing cell density were constructed (in Gambit) and a grid of 80,327 tetrahedral cells was found to give an essentially grid-independent solution. That is, the predicted maximum velocity using a grid twice as dense was only 3% higher than that for the grid of 80,327 cells (Fig. 5). The number of time steps over one breathing cycle was also increased systematically and it was found that the flow at a specific time was virtually independent of the number of time steps (Fig. 5). This confirms that alveolar flow is essentially quasi steady.

The flow field produced by FLUENT was saved to disk at each time step along with the grid at that time (the grid was expanding and contracting over the breathing cycle). Instantaneous streamlines were computed as fluid particle tracks in the flow field frozen at a particular time using Tecplot 360 2011 (Bellevue, WA, USA). In Tecplot, particle positions are advanced by performing a Runge-Kutta integration of the velocity field with linear interpolation between nodes and solution time levels.

Results

The typical structure of flow patterns in the midplane (symmetric) of the alveolar cavity is shown in Fig. 6. Four different zones can be defined.

Zone I is defined as that part of the flow which undergoes recirculation or spirals in the middle of the alveolar cavity (shown in red in Fig. 6). Zone II (shown in blue) is a product of the expansion/contraction of the alveoli and includes flows that enter the alveolus from the central channel during inspiration and leave the alveolus and return to the central channel during expiration. These convective communications occur through the distal side of the alveolar opening. The incoming/outgoing flows wrap around the rotating/spiral flow of zone I their streamlines terminate at the cavity wall. Zone III (marked in green) is similar to zone II only in this case streamlines approach the proximal end of the alveolus wall entering the alveolus between the proximal corner and the stagnation point. This small zone appears only in case a stagnation point is present in the flow near the proximal corner of the opening of the alveolus (all generations except the 23rd). Zone IV (marked in black) includes streamlines which pass over the alveolus mouth and feed the many other alveoli located downstream. We note that zones I and IV are clearly visible in the flow in the cluster of alveoli derived from the imaged lung (Fig. 3).

The foregoing results shown in Fig. 6 were also studied in the past (see, for instance, Tsuda et al. [6]) but, until now, the off-midplane structure has remained largely unexplored. Our preliminary computations of flow in a realistic alveolated duct model (Fig. 3) suggested that the off-midplane flow has a rich and complex structure. The instantaneous streamlines at maximum inspiratory flow in our model of *moving* walls (Fig. 7) reveal that closed orbits exist at the symmetry plane $x = 0$, whereas off this plane the

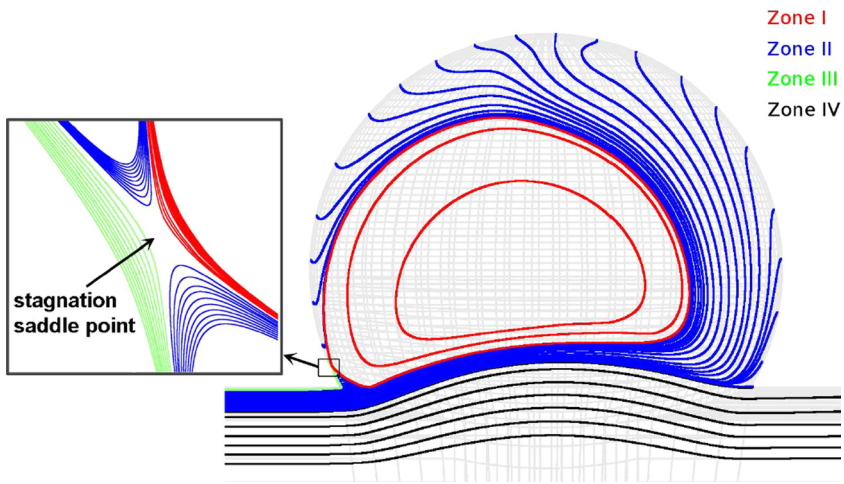

Fig. 6 Flow in the midplane of an idealized spherical alveolus showing the four distinct zones and the stagnation point. Zone I, the rotating flow, which has closed streamlines, in the middle of the alveolus. Zone II, the flow that enters the alveolus distally from the duct. Zone III, the small amount of flow that enters the alveolus from the duct proximally and is between the alveolar wall and the stagnation point. Zone IV, the duct flow that passes by the alveolus. (Note that this flow was produced using the same finite element CFD code used to compute the flow shown in Fig. 3.)

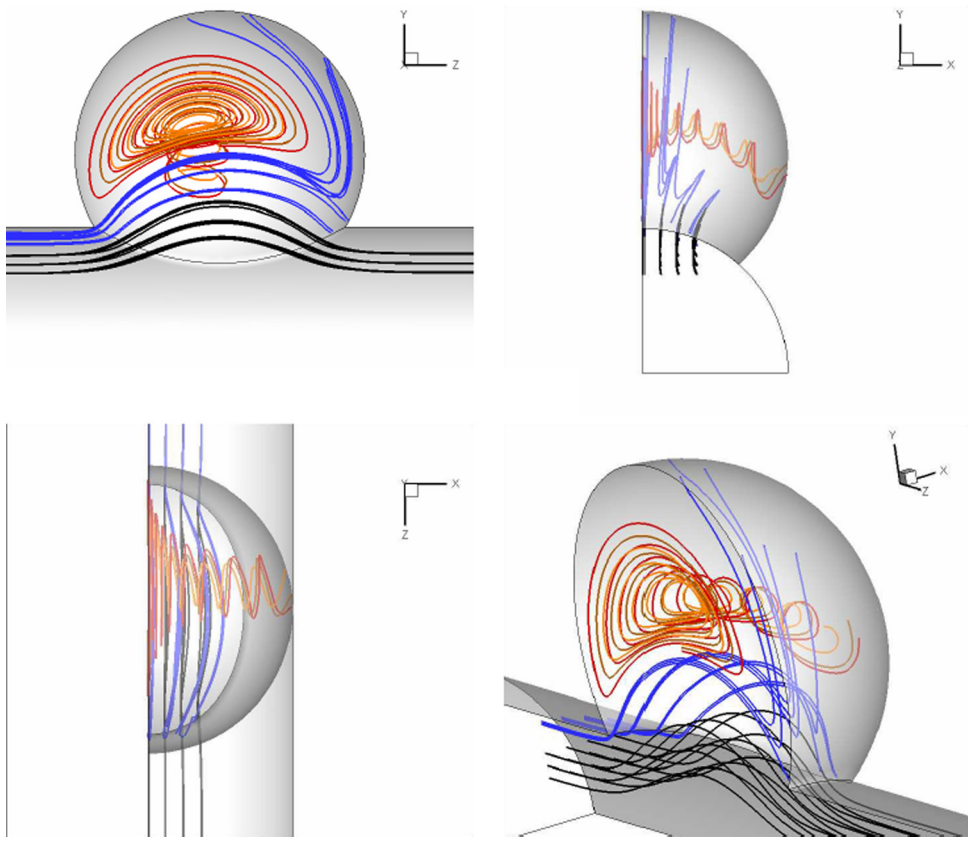

Fig. 7 Instantaneous streamlines originating off midplane of an idealized spherical alveolus at maximum inspiratory flow ($t = T/4$) for conditions typical of generation 18 ($Q_A/Q_D = 0.0021$ and $Re_{max} = 0.25$). Zones comparable to zones I, II, and IV are clearly discernible but the streamlines in zone I spiral towards the alveolar wall; one inside the other, like a Russian nesting doll. (The structure of the flow is such that zone III must exist but it was too small to be visualized in these figures.)

flow spirals towards the wall. Note that these result differ from the results of Pozrikidis [40], who dealt with Stokes flow over a rigid nonmoving spherical indentation and found nested closed streamlines off the symmetry plane too.

Inspection of the streamlines in Fig. 7 reveals that off midplane there are the same distinct zones as found in the midplane. That is, in the middle of the alveolus a rotating flow exists only now the streamlines spiral towards the sidewall, creating a funnel-like

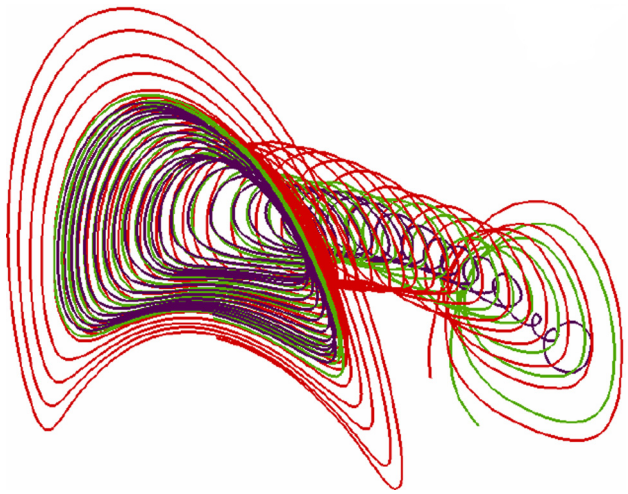

Fig. 8 Details of Russian-nesting-doll structure. $Q_A/Q_D = 0.0003$, $Re_{max} = 2.0$, $t = T/4$.

zone (zone I). Surrounding the center flow (zone I) is a region of flow that enters the alveolus distally from the duct (zone II). While not visible in Fig. 7, there would also be a small amount of duct flow entering the alveolus proximally, between the wall and the stagnation point (zone III). Finally, the majority of the duct flow passes by the alveolus (zone IV).

We note that at each instant in time all zones appear to be convectively separated; that is, the streamlines in one zone do not cross into another. Also, because the wall is expanding (in inspiration), all streamlines in the alveolus terminate at the wall. (We note that eventually all streamlines terminate either on the wall of the duct or of a more distal alveolus.) The exception is in the midplane, where the streamlines are closed; and hence do not terminate at the wall.

Closer inspection of zone I (Fig. 8) shows that the flow in this region is composed of separate funnel-like subregions, each convectively separated. That is, the spiraling streamlines are arranged one inside the other, reminiscent of a Russian nesting doll. We note that zone I exists on both sides of the midplane in which the streamlines are closed, and each half of zone I spirals to the nearest sidewall.

Henry and Tsuda [10] showed that rotational flow occurs to some degree in all but the terminal alveolar ducts. Our current results confirm that there is no rotation in the flow of the alveoli on the terminal ducts (Fig. 9). It appears that the Russian-doll structure occurs in all alveoli except the terminal alveolar duct (Fig. 9); that is, in all alveoli in which there are closed streamlines in the midplane. Our current results also confirm that the magnitude of the local velocity in the alveolus is a small fraction of that in the duct (Fig. 9 lower right panel). It is also evident (Fig. 9 lower right panel) that the local maximum velocity in the alveolus reduces approximately linearly with distance from the midplane.

It is noted that instantaneous streamlines are only a snap shot of the flow and as such they cannot readily shed light on the dynamics of the flow. In reality, the alveolus is expanding and contracting and even though these flows have only a small amount of inertia it is sufficient to ensure that the flow in expiration is not an exact replica in reverse of the flow in inspiration (Henry et al. [8]). This is most noticeable in the difference in shape and position of zone I in inspiration and expiration for alveolar flow in the entrance region of the acinus (Fig. 10).

The change in shape and position of zone I over the breathing cycle forces commensurate changes in zone II. Hence, the interaction between zone I and zone II is time dependent (due to nonzero inertia effects [8]) and this may lead to alveolar residual air (zone I) mixing with incoming/outgoing air (zone II). This off-midplane interaction is a possible new mechanism of convective mixing [9,11].

Finally, we calculated a few exploratory fluid particle tracks over several breathing cycles to confirm that fluid particles follow paths similar to the streamlines. We first released four particles near the proximal corner of the alveolus (Fig. 11), which is the region in which particle-laden flow enters the alveolus from the duct [10]. The three particles further away from the alveolar wall followed paths that resembled the streamlines seen in Fig. 9; that is, the particles traveled in nested spiral paths from the midplane towards the wall. Once in near proximity to the wall, they traveled along the wall and back towards the midplane, again in a spiral pattern. Eventually, after 11–13 breaths, orbits of all three particles came very closed to the wall within a radius of the particles so that they deposited by interception [41]. (We note that no intrinsic motion is involved in this simulation. With simultaneous action of intrinsic motion, such as Brownian motion, particles with even very small intrinsic motion would deposit once their orbits are within an effective range from the walls.) The particle released nearest the wall (Fig. 11, lower panels) remained close to the wall, staying roughly in the plane of its release, and deposited by interception in the second cycle.

We then release four particles near the center of the alveolus (Fig. 12). Three particles followed a trend similar to the three particles discussed above in that they traveled in nested spiral paths from the midplane towards the wall, and then traveled along the wall and back towards the midplane. After between 8 and 14 breathing cycles all three particles deposited by interception. The particle that was released closest to the alveolus entrance (Fig. 12, lower panels) followed a slightly different path in that it first stayed near the midplane. While close to the midplane the particle reduced the size of its orbit with each revolution but eventually drifted away from the midplane. The particle then approached the sidewall and deposited, after 11 breaths. Unlike the other three particles, this particle deposited without first traveling along the wall in the direction of the midplane.

Discussion and Summary

The predicted streamline patterns in the symmetric plane of a spherical alveolus (Fig. 6) match those previously predicted using axisymmetric models [6,8] and a 3D Stokes model [7]. Extending our study away from the midplane, we show that the recirculating flow identified in the middle of the alveolar cavity changes into a spiraling off-center flow enhancing the interaction between ductal incoming flow and the fluid occupying the space inside the alveolus. The character of the flow in the model alveoli is largely controlled by the value of Q_A/Q_D. As we have assumed that the geometry remains similar at all times, Q_A/Q_D is simply a function of model geometry. Specifically, $Q_A/Q_D = V_A/V_D$, where V_A is the volume of the alveolus. We have found previously (see Henry and Tsuda [10], for instance) that the strength of the rotation of the flow in the alveolus is inversely proportional to the value of Q_A/Q_D. Indeed, above a certain value of Q_A/Q_D the alveolar flow does not rotate. In addition, the strongest rotation occurs is alveoli in the entrance generations of the acinus.

Our predictions show that significant information about the flow in actual alveoli can be gained from studying the flow in an idealized spherical model alveolus. This fact[2] itself indicates that the exact shape of the alveolus appears to have a relatively minor influence on the presence of the alveolar recirculation. Furthermore, we have specifically shown that the flow in the spherical-alveolus model has the same general characteristics as the flow in a model of a cluster of alveoli generated from images of actual rat's lungs (Fig. 3). In both cases, there exists in the middle of the alveolar cavity a rotating flow that spirals from the midplane to the sidewalls (zone I). These spiral patterns form a funnel-like

[2]In addition, calculations in rigid versions of both models were also shown to share similar characteristics; i.e., a rotating flow in the alveolus separated from the duct flow by a stream surface as we have reported previously (e.g., Tsuda et al. [6]; Haber et al. [7,41]; Henry et al. [8–10]).

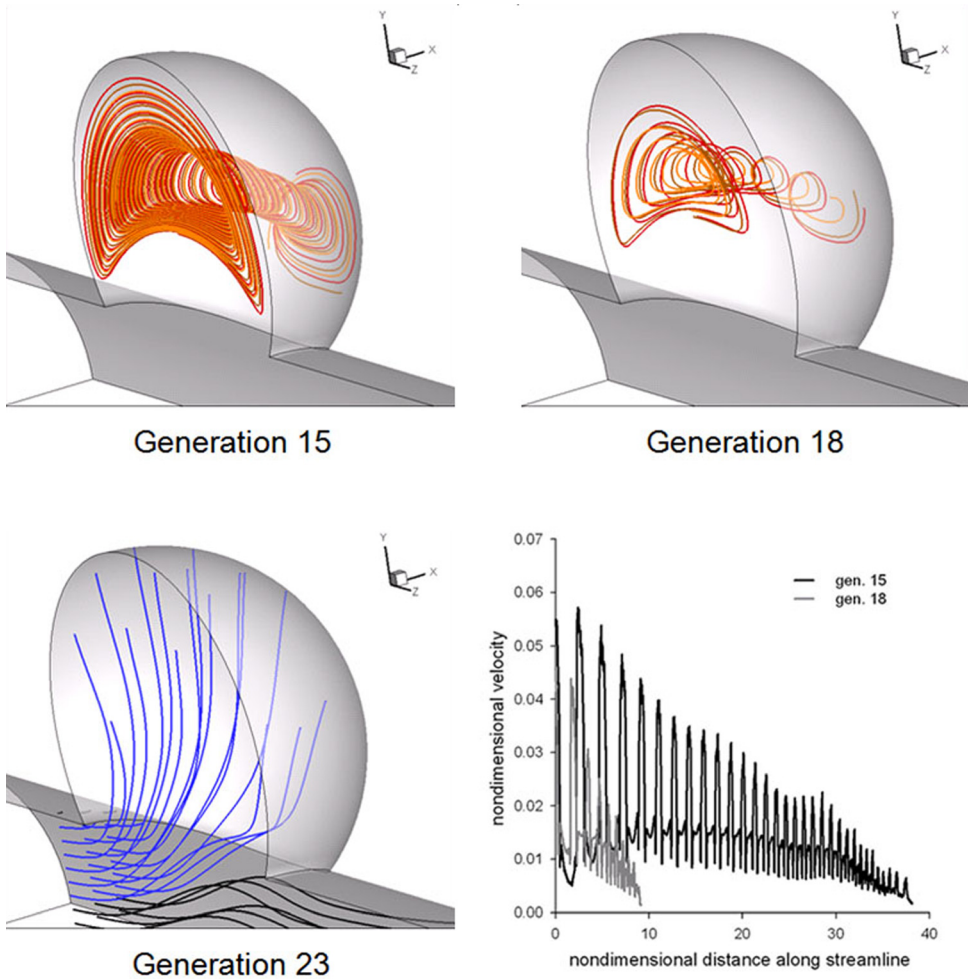

Fig. 9 Instantaneous streamlines at maximum inspiratory flow ($t = T/4$) for alveoli located in generations 15, 18, and 23. Q_A/Q_D and $Re_{max} = 0.0003$ and 2.0, 0.0021 and 0.25, and 0.25 and 0.008, for the mentioned generations, respectively. Lower right panel: Velocity magnitude along representative streamlines. Velocity normalized by the mean velocity in the duct and distance normalized by the duct diameter. Velocity curves represent the velocity along the outermost streamline, shown in red, in the upper panels.

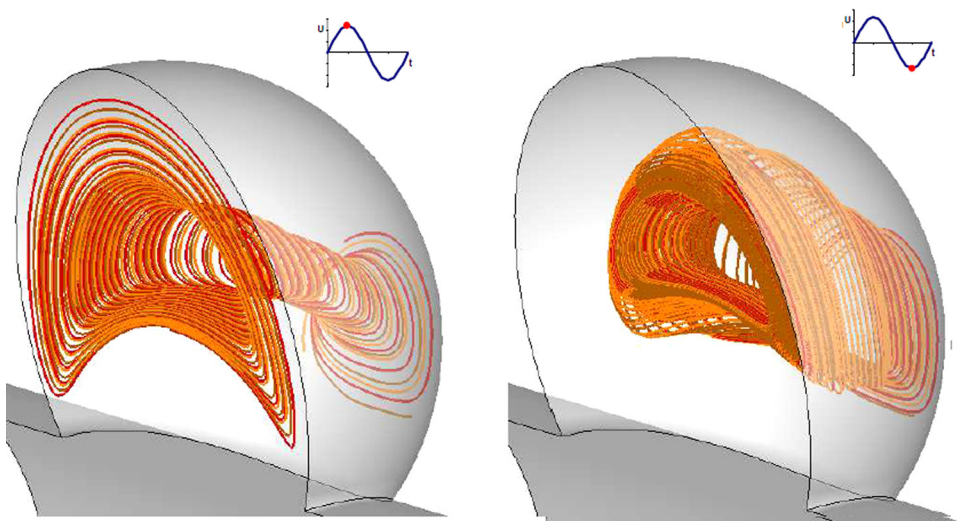

Fig. 10 Instantaneous streamlines in zone I originating off midplane of an idealized spherical alveolus for conditions typical of generation 15 ($Q_A/Q_D = 0.0003$ and $Re_{max} = 2.0$). Left panel: Maximum inspiratory flow ($t = T/4$). Right panel: Maximum expiratory flow ($t = 3\,T/4$).

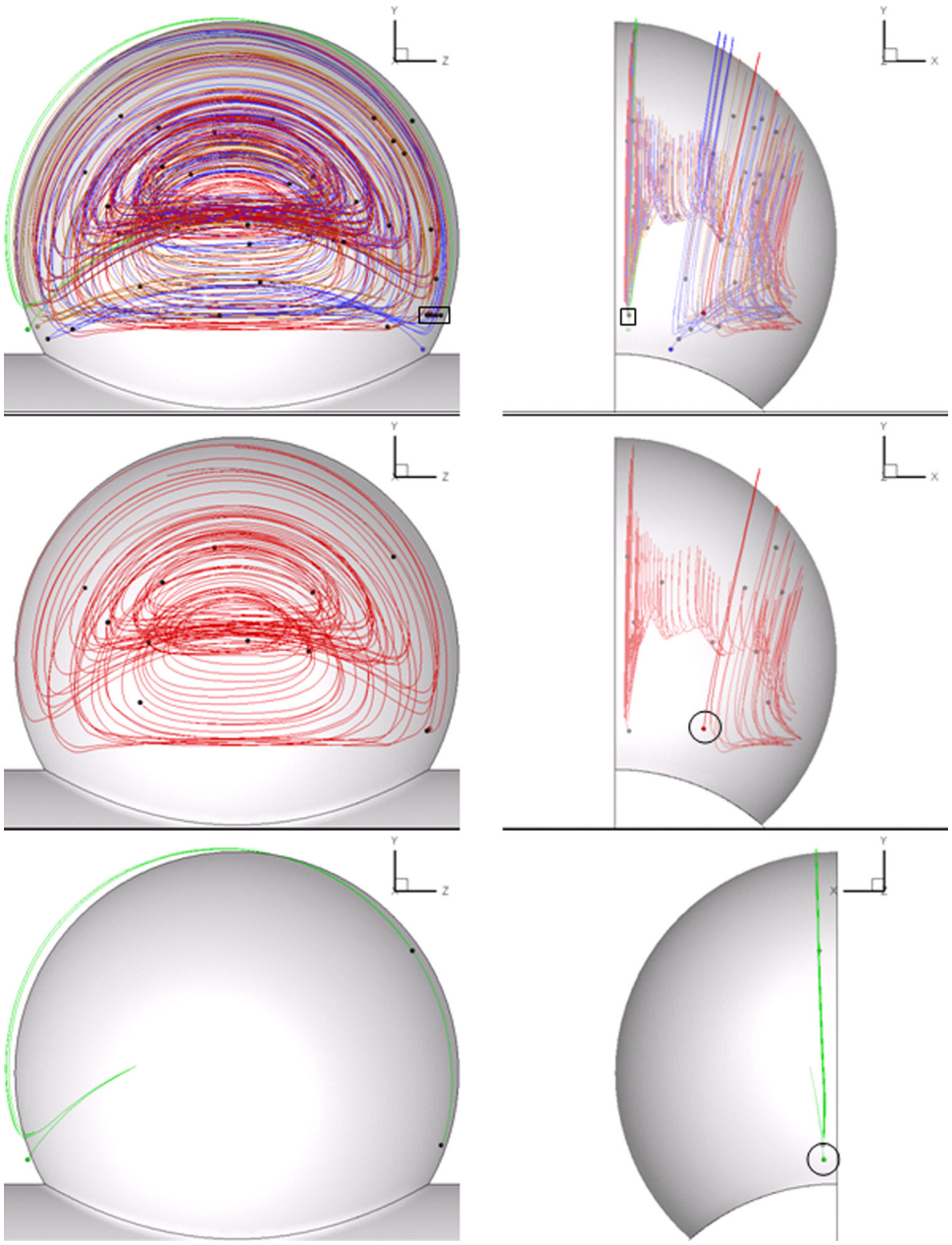

Fig. 11 Four particles released at the beginning of inspiration near the distal corner of the alveolus near the symmetry plane (shown encircled by a small black rectangle in the top left panel and by a small black square in the top right panel) and tracked over multiple breaths (top panels). $Q_A/Q_D = 0.0003$, $Re_{max} = 2.0$, $t = T/4$. Each track is depicted in a different color. The final (deposited) positions of two selected tracks are shown by open circles in the middle and lower right panels. The small closed circles indicate the position of the particle at the end of each breathing cycle. (Geometry shown at minimum volume.)

structure with similar structures of increasingly smaller size one inside the other, like a Russian nesting doll, and the central duct flow enters the alveolus with an amount given as Q_A through the distal part of the alveolar opening (zone II) wrapping around these Russian-doll-like structures (zone I). We have also shown that fluid particles (Figs. 11 and 12) tend to follow similar paths to that of the streamlines (Figs. 7 and 8). That is, their tracks form nested, funnel-like, structures. The particles first move towards the central region of the alveolus while staying close to the symmetry plane and then travel away from the symmetry plane and towards the sidewalls, where they eventually deposit by interception.

We have shown that on the midplane of a spherical alveolus the streamlines in the recirculating region are closed (Fig. 6). We have also seen that on either side of the midplane, the streamlines in zone I spiral to the wall (Fig. 7). Hence, it can to be concluded that the midplane of the flow in a spherical alveolus is a singular plane. This plane in infinitesimally thin, a streamline starting only a small distance away from the midplane will eventually move away from the plane.

An important question related to the effectiveness of convective mixing, is how the particle-laden air entering the alveolus from the duct (zone II) mixes with the residual air, which is mostly in the recirculation region (zone I). We have shown (Fig. 10) that zone I changes position and shape over the breathing cycle because the duct flow has some small but nonzero inertia. The time-dependent nature of the position and size of zone I likely

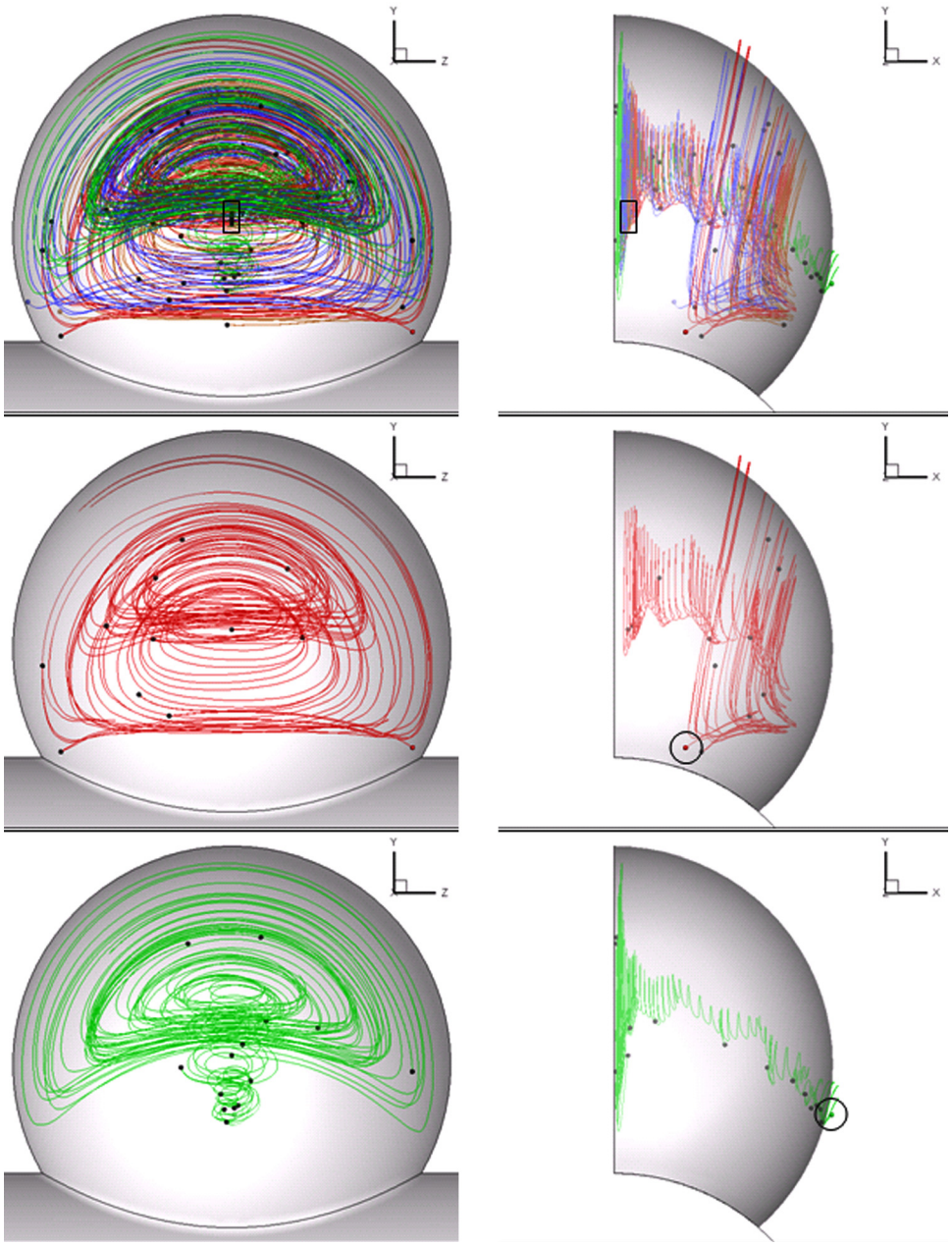

Fig. 12 Four particles released at the beginning of inspiration in the center of the flow near the symmetry plane (shown encircled by small black rectangles in the top panels) and tracked over multiple breaths (top panels). $Q_A/Q_D = 0.0003$, $Re_{max} = 2.0$, $t = T/4$. Each track is depicted in a different color. The final (deposited) positions of two selected tracks are shown by open circles in the middle and lower right panels. The small closed circles indicate the position of the particle at the end of each breathing cycle. (Geometry shown at minimum volume.)

encourages convective mixing between zone I and zone II. Thus, each alveolus may be considered an efficient mixing unit comprising the mixing region of the Russian-doll structure, zone I, and the feeder region, zone II, which wraps around zone I.

Turning our attention to the acinar tree. Due to the linearity of the Stokes equations that govern the flow approximately, it is obvious that the strength of rotation of zone I is directly related to the flow strength in the duct Q_D (and hence Q_A/Q_D). Therefore, as the flow rate in the duct is proportional to the acinar volume distal of the alveolus of interest ($Q_A/Q_D = V_A/V_D$), the rotational strength of zone I in an individual alveolus will decrease as the terminal ducts are approached. Hence, in general, the further from the acinar entrance, the larger Q_A/Q_D and the smaller the amount of mixing in the individual alveoli. It should be noted, however, that this view is based on the assumption that the acinar tree is perfectly symmetric, i.e., a symmetric division of flow from one generation to the next. In practice, the acinar tree is asymmetric; which results in there being a range of path lengths to the terminal sacs. This feature of an actual acinus can result in a significant variation of Q_A/Q_D in a generation; and hence, a significant variation in mixing in one generation, depending on the path taken.

The physiological implications of viewing the alveolus as mixer-feeder unit are many. First, classical theory claims there can be no mixing of particles but the mixer-feeder view of alveolar flow provides a mechanism for convective mixing [9,11]. Second, as the strength of the mixer-feeder unit is related to Q_A/Q_D the effectiveness of each unit varies over each generation. Consideration of the distribution of Q_A/Q_D in the acinar tree, together

with designing the optimal particle size and shape, is important in establishing an effective strategy for therapeutic drug delivery. Similar consideration is necessary to access accurately the local burden of adverse particle effects causing tissue injury in the case of deposition in the lung parenchyma. Third, in the postnatally developing lung, mixing and deposition of submicron particles in the pulmonary acinus must be age dependent. This is because structural change (alveolation) is the major event in postnatal lung development; the newborn human acinus is largely saccular with few alveoli; and hence, few mixer-feeder units, rapid bulk structural alveolation occurs in the first 2–3 years of life [42]. Accordingly, the pattern of deposition of submicron particles in the infant lung is dramatically age dependent, and must be different from that in the fully developed adult lung. Our idea of "mixer-feeder" has therefore important implications for drug delivery and lung injury estimates in infants.

Acknowledgment

We thank Marco Stampanoni, Federica Marone, and Christoph Hintermüller for their professional support at the beamline TOMCAT at the Swiss Light Source and Mohammed Ouanella for technical assistance. Dr. Henry would like to thank Dr. Mohammad Naraghi, Chair of Mechanical Engineering, Manhattan College, NY, for making available Gambit, Fluent, and Tecplot, and for the use of the department's computing facilities. This work was supported in part by the Swiss National Science Foundation Grant 3100A0-109874/1 and 310030-125397/1 and National Heart, Lung, and Blood Institute Grants, HL070542, HL074022, HL094567, HL054885.

References

[1] Haefeli-Bleuer, B., and Weibel, E. R., 1988, "Morphometry of the Human Pulmonary Acinus," Anatomical Rec., **220**(4), pp. 401–414.
[2] ICRP Publication 66, 1994, "Human Respiratory Tract Model for Radiological Protection," A report of a Task Group of the International Commission on Radiological Protection, Ann. ICRP, **24**(1–3), pp. 1–482.
[3] Tsuda, A., Otani, Y., and Butler, J. P., 1999, "Acinar Flow Irreversibility Caused by Boundary Perturbation of Reversible Alveolar Wall Motion," J. Appl. Physiol., **86**(3), pp. 977–984.
[4] Tsuda, A., Rogers, R. A., Hydon, P. E., and Butler, J. P., 2002, "Chaotic Mixing Deep in the Lung," Proc. Natl. Acad. Sci. U.S.A., **99**, pp. 10173–10178.
[5] Tippe, A., and Tsuda, A., 2000, "Recirculating Flow in an Expanding Alveolar Model: Experimental Evidence of Flow-Induced Mixing of Aerosols in the Pulmonary Acinus," J. Aerosol Sci., **31**(8), pp. 979–986.
[6] Tsuda, A., Henry, F. S., and Butler, J. P., 1995, "Chaotic Mixing of Alveolated Duct Flow in Rhythmically Expanding Pulmonary Acinus," J. Appl. Physiol., **79**(3), pp. 1055–1063.
[7] Haber, S., Butler, J. P., Brenner, H., Emanuel, I., and Tsuda, A., 2000, "Flow Field in Self-Similar Expansion on a Pulmonary Alveolus During Rhythmical Breathing," J. Fluid Mech., **405**, pp. 243–268.
[8] Henry, F. S., Butler, J. P., and Tsuda, A., 2002, "Kinematically Irreversible Flow and Aerosol Transport in the Pulmonary Acinus: A Departure From Classical Dispersive Transport," J. Appl. Physiol., **92**, pp. 835–845.
[9] Henry, F. S., Laine-Pearson, F. E., and Tsuda, A., 2009, "Hamiltonian Chaos in a Model Alveolus," ASME J. Biomech. Eng., **131**(1), p. 011006.
[10] Henry, F. S., and Tsuda, A., 2010, "Radial Transport Along the Human Acinar Tree," ASME J. Biomech. Eng., **132**(10), p. 101001.
[11] Tsuda, A., Laine-Pearson, F. E., and Hydon, P. E., 2011, "Why Chaotic Mixing of Particles Is Inevitable in the Deep Lung," J. Theor. Biol., **286**, pp. 57–66.
[12] Berg, E. J., Weisman, J. L., Oldham, M. J., and Robinson, R. J., 2010, "Flow Field Analysis in a Compliant Acinus Replica Model Using Particle Image Velocimetry (PIV)," J. Biomech., **43**(6), pp. 1039–1047.
[13] Berg, E. J., and Robinson, R. J., 2011, "Stereoscopic Particle Image Velocimetry Analysis of Healthy and Emphysemic Alveolar Sac Models," J. Biomech. Eng., **133**(6), p. 061004.
[14] Chhabra, S., and Prasad, A. K., 2010, "Flow and Particle Dispersion in a Pulmonary Alveolus—Part I: Velocity Measurements and Convective Particle Transport," J. Biomech. Eng., **132**(5), p. 051009.
[15] Chhabra, S., and Prasad, A. K., 2010, "Flow and Particle Dispersion in a Pulmonary Alveolus—Part II: Effect of Gravity on Particle Transport," J. Biomech. Eng., **132**(5), p. 051010.
[16] Oakes, J. M., Day, S., Weinstein, S. J., and Robinson, R. J., 2010, "Flow Field Analysis in Expanding Healthy and Emphysematous Alveolar Models Using Particle Image Velocimetry," J. Biomech. Eng., **132**(2), p. 021008.
[17] Harding, E. M., Jr., and Robinson, R. J., 2010, "Flow in a Terminal Alveolar Sac Model With Expanding Walls Using Computational Fluid Dynamics," Inhal. Toxicol., **22**(8), pp. 669–678.
[18] Kumar, H., Tawhai, M. H., Hoffman, E. A., and Lin, C. L., 2009, "The Effects of Geometry on Airflow in the Acinar Region of the Human Lung," J. Biomech., **42**(11), pp. 1635–1642.
[19] Kumar, H., Tawhai, M. H., Hoffman, E. A., and Lin, C. L., 2011, "Steady Streaming: A Key Mixing Mechanism in Low-Reynolds-Number Acinar Flows," Phys. Fluids, **23**(4), p. 041902.
[20] Ma, B., and Darquenne, C., 2011, "Aerosol Deposition Characteristics in Distal Acinar Airways Under Cyclic Breathing Conditions," J. Appl. Physiol., **110**(5), pp. 1271–1282.
[21] Sznitman, J., Heimsch, F., Heimsch, T., Rusch, D., and Rosgen, T., 2007, "Three-Dimensional Convective Alveolar Flow Induced by Rhythmic Breathing Motion of the Pulmonary Acinus," ASME J. Biomech. Eng., **129**, 658–665.
[22] Sznitman, J., Heimsch, T., Wildhaber, J. H., Tsuda, A., and Rösgen, T., 2009, "Respiratory Flow Phenomena and Gravitational Sedimentation in a Three-Dimensional Space-Filling Model of the Pulmonary Acinar Tree," ASME J. Biomech. Eng., **131**(3), p. 031010.
[23] Davies, C. N., 1972, "Breathing of Half-Micron Aerosols: II Interpretation of Experimental Results," J. Appl. Physiol., **35**, pp. 605–611.
[24] Taylor, G. I., 1967, *Low Reynolds Number Flow*, The National Committee for Fluid Mechanics Film, Encyclopaedia Britanica Education Corporation.
[25] Davidson, M. R., and Fitz-Gerald, J. M., 1972, "Flow Patterns in Models of Small Airway Units of the Lung," J. Fluid Mech., **52**, pp. 161–177.
[26] Filipovic, N., Haberthür, D., Henry, F. S., Milasinovic, D., Nikolic, D., Schittny, J., and Tsuda, A., 2010, "Recirculation Identified in a 3D Alveolar Duct Reconstructed Using Synchrotron Radiation Based X-Ray Tomographic Microscopy," ATS meeting, New Orleans (abstr.).
[27] Filipovic, N., Henry, F. S., Milasinovic, D., and Tsuda, A., 2011, "Can Complex Alveolar Flow Patterns in Off Mid-Plane Trap Aerosol Particles?," ATS meeting, Denver (abstr.).
[28] Tsuda, A., Filipovic, N., Haberthür, D., Dickie, R., Matsui, Y., Stampanoni, M., and Schittny, J. C., 2008, "Finite Element 3D Reconstruction of the Pulmonary Acinus Imaged by Synchrotron X-Ray Tomography," J. Appl. Physiol., **105**(3), pp. 964–976.
[29] Haberthür, D., Hintermüller, C., Marone, F., Schittny, J. C., and Stampanoni, M., 2010, "Radiation Dose Optimized Lateral Expansion of the Field of View in Synchrotron Radiation X-Ray Tomographic Microscopy," J. Synchrotron Radiat., **17**(5), pp. 590–599.
[30] Sznitman, J., Sutter, R., Altorfer, D., Stampanoni, M., Rösgen, T., and Schittny, J. C., 2010, "Visualization of Respiratory Flows From 3D Reconstructed Alveolar Airspaces Using X-Ray Tomographic Microscopy," J. Visualization, **14**(4), pp. 337–345.
[31] Tschanz, S. A., Makanya, A. N., Haenni, B., and Burri, P. H., 2003, "Effects of Neonatal High-Dose Short-Term Glucocorticoid Treatment on the Lung: A Morphologic and Morphometric Study in the Rat," Pediatr. Res., **53**(1), pp. 72–80.
[32] Luyet, C., Burri, P. H., and Schittny, J. C., 2002, "Suppression of Cell Proliferation and Programmed Cell Death by Dexamethasone During Postnatal Lung Development," Am. J. Physiol. Lung Cellular Mol. Physiol., **282**(3), pp. 477–483.
[33] Stampanoni, M., Groso, A., Isenegger, G., Mikuljan, G., Chen, Q., Bertrand, A., Henein, S., Betemps, R., Frommherz, U., Böher, P., Meister, D., Lange, M., and Abela, R., 2006, "Trends in Synchrotron-Based Tomographic Imaging: The SLS Experience," Proc. SPIE, **6318**, p. 63180M.
[34] Filipovic, N., Mijailovic, S., Tsuda, A., and Kojic, M., 2006, "An Implicit Algorithm Within the Arbitrary Lagrangian-Eulerian Formulation for Solving Incompressible Fluid Flow With Large Boundary Motions," Comp. Methods Appl. Mech. Eng., **195**, pp. 6347–6361.
[35] Haber, S., Yitzhak, D., and Tsuda, A., 2003, "Gravitational Deposition in a Rhythmically Expanding and Contracting Alveolus," J. Appl. Physiol., **95**, pp. 657–671.
[36] Pedley, T. J., Schroter, R. C., and Sudlow, M. F., 1977, "Gas Flow and Mixing in the Airways," in *Bioengineering Aspects of the Lung*, edited by J. B. West, Marcel Dekker, New York.
[37] Weibel, E. R., Sapoval, B., and Filoche, M., 2005, "Design of Peripheral Airways for Efficient Gas Exchange," Respir. Physiol. Neurobiol., **148**(1–2), pp. 3–21.
[38] Weibel, E. R., 1963, *Morphometry of the Human Lung*, Springer/Academic, Heidelberg.
[39] White, F. M., 1974, *Viscous Fluid Flow*, McGraw-Hill, New York.
[40] Pozrikidis, C., 1994, "Shear Flow Over a Plane Wall With an Axisymmetric Cavity or a Circular Orifice of Finite Thickness," Phys. Fluids, **6**, pp. 68–79.
[41] Haber, S., Yitzhak, D., and Tsuda, A., 2010, "Trajectories and Deposition Sites of Spherical Particles Moving Inside Rhythmically Expanding Alveoli Under Gravity-Free Conditions," J. Aerosol. Med. Pulm. Drug Deliv., **23**(6), pp. 405–413.
[42] Semmler-Behnke, M., Kreyling, W. G., Schulz, H., Takenaka, S., Butler, J. P., Henry, F. S., and Tsuda, A., 2012, "Nanoparticle Delivery in Infant Lungs," Proc. Natl. Acad. Sci. U.S.A., **109**(13), pp. 5092–5097.